The Influence of Alloy Composition on Precipitates of the Al-Mg-Si System
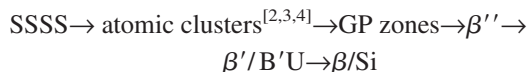
C.D. MARIOARA, S.J. ANDERSEN, H.W. ZANDBERGEN, and R. HOLMESTAD

To study how changes in solute elements affect precipitation, six Al-Mg-Si alloys aged at 175 °C were investigated by transmission electron microscopy (TEM). In alloys with 1.3 at. pct solute, when the Si/Mg ratio exceeds 5/6, a sharp hardness peak appears after 3 hours that correlates with a high density of fine Guinier–Preston (GP) zones. A second, broader peak correlates with β'' precipitates and U phases. With high Si/Mg ratios, GP zones survive for long aging times. The β''-Mg_5Si_6 phase becomes very stable in the alloy with its Si/Mg ratio closest to 6/5. Deviation from this ratio increases fractions of β', U-phases and disordered precipitates. In Mg-rich alloys less GP zones form and the first peak is suppressed. A coarse precipitate microstructure of β'' and β' develops, the volume fraction being much higher than in Si-rich alloys. The Mg-rich alloys overage faster. Reducing the content of solutes causes alloys with high Si/Mg ratios to have a more Mg-rich behavior.

I. INTRODUCTION

THE Al-Mg-Si heat-treatable alloys are characterized by a large increase in hardness upon aging. The strength increase is caused by interface strain between the matrix and small, semicoherent, metastable precipitates forming from solid solution. In the Al-Mg-Si system, many high-quality alloys have been developed having attractive properties for manufacturers of a variety of goods. Factors such as low price, low density, high weldability, medium strength, high extrudability, and good corrosive properties have supported a continuous growth in the usage and production of these alloys. Today more than 90 pct of the extruded Al goods in Western Europe are based on the 6xxx series.[1]

For a long time, transmission electron microscopy (TEM) has been among the most significant techniques in the investigation of the microstructure in these materials. A considerable amount of research has been invested on studies of the precipitates and how they influence the material properties. Even with the newest generation of high-resolution electron microscopes (HREMs), many of the questions have been difficult to answer. In part, this is caused by the complex thermal processing of these alloy systems in general, with several processing steps that each may influence the type of precipitate, its distribution, and size. The smallness of the individual precipitates makes them difficult to study. Until quite recently, very few details concerning precipitate structures were available. A deeper level of understanding is now made possible as more phases have been discovered and the crystal structures of many of the phases of the precipitation sequence have been solved.

$$SSSS \rightarrow \text{atomic clusters}^{[2,3,4]} \rightarrow \text{GP zones} \rightarrow \beta'' \rightarrow$$
$$\beta'/B'U \rightarrow \beta/Si$$

C.D. MARIOARA, Research Scientist, and S.J. ANDERSEN, Senior Scientist, are with SINTEF Materials and Chemistry, N-7465 Trondheim, Norway. Contact e-mail: calin.d.marioara@sintef.no H.W. ZANDBERGEN, Professor, is with the National Centre for HREM, Laboratory of Materials Science, Delft University of Technology, 2628 AL Delft, The Netherlands. R. HOLMESTAD, Professor, is with the Department of Physics, Norwegian University of Science and Technology, N-7491 Trondheim, Norway.
Manuscript submitted January 23, 2004.

Table I gives references and more data for these phases. The GP zones and β'' have similar unit cells and monoclinic structures. The terms U1, U2, and B' are also called A, B, and C.[5,6] The U1 and U2 phases were recently solved;[7,8] U2 is a common precipitate. It is orthorhombic with composition AlMgSi. It is structurally related to both β' and β''. U1 is trigonal and has composition $MgAl_2Si_2$. Plates of Si appear in Al-Mg-Si alloys rich in silicon. Except for β and Si, all phases have needle-shaped morphology, with the long dimension coherent with a <100> direction of Al.

The alloy composition and thermal history determine the final precipitate microstructure in a sample, *i.e.*, type, size, amount, and distribution of precipitates. Typically, Al-Mg-Si alloys are homogenized, extruded, and quickly cooled to—and stored at—room temperature (RT) for a few hours before the final aging treatment. During the extrusion procedure, the temperature is usually above 400 °C, but it may reach 500 °C for a short while, and normally, all solute became redissolved in the matrix. To avoid the nucleation and growth of incoherent Mg-Si phases during cooling, a high cooling rate to RT is important.

Such rapid cooling also produces a supersaturated solid solution of Mg and Si together with a high vacancy concentration. This is a potent mix that is a prerequisite for a strong precipitation-hardened alloy.

The RT storage prior to aging is necessary for practical reasons. It has a significant effect on the precipitate microstructure.[9] A long storage time commonly produces a coarser final microstructure in Si-rich alloys. For a 6082 (T6) alloy, this results in lower strength. For reduced alloy content or Mg-rich alloys, the situation may be reversed.

The aging heat treatment of the extrusions is performed for 4 to 8 hours at a temperature between 165 °C and 185 °C, until maximum hardness is achieved—the so-called *T6* condition. Aging temperature and time[9] determine sizes and number densities of the hardening precipitates (mainly GP zones and β''). Using a higher temperature, less time is required to reach the T6 condition, but a coarser, lower-hardness precipitate microstructure is developed. The strength of an alloy is closely connected to the sizes, number densities, and volume fractions of the metastable phases.[9,10,11]

Table I. Overview of Known Precipitation Phases in Al-Mg-Si; U1, U2, and B′ Are Also Called A, B, and C[5,6]

Phase	Shape	Compound	Space Group	Lattice Parameters (nm)
GP zones[13,15]	needle	unknown	$C2/m$	$a = 1.48$, $b = 0.405$, $c = 0.648$, $\beta = 105.3$ deg
β''[12,13]	needle	Mg_5Si_6	$C2/m$	$a = 1.516$, $b = 0.405$, $c = 0.674$, $\beta = 105.3$ deg
β'[7,17]	needle	$Mg_{1.8}Si$	$P6_3$	$a = b = 0.715$, $c = 0.405$, $\gamma = 120$ deg
U1[5–8]	needle	$MgAl_2Si_2$	$P\bar{3}m1$	$a = b = 0.405$, $c = 0.674$, $\gamma = 120$ deg
U2[5–8,17]	needle	$MgAlSi$	P_{nma}	$a = 0.675$, $b = 0.405$, $c = 0.794$
B′[5]	lath	unknown	hexagonal	$a = 1.04$, $c = 0.405$, $\gamma = 120$ deg
β	plate	Mg_2Si	$F_{m\bar{3}m}$	$a = 0.6354$
Si	plate	Si	F_d3m	$a = 0.5431$

Quantification of these phases for different compositions and thermal histories is therefore important. Without a proper quantification, one cannot hope to reach a thorough understanding of the material properties of these materials, let alone make valid predictions using computer simulations.

The present work is focused on how alloy composition affects the precipitate microstructure and hardness. A temperature of 175 °C was chosen for the isothermal heat treatment. This temperature is commonly used in industry and will cause β'' to precipitate. β'' is the most efficient hardening phase in this alloy system and forms between 125 °C and 200 °C. The composition of β'' is Mg_5Si_6,[12,13] and therefore, the Mg/Si ratio of 5/6 was set as an important reference for the composition of the alloys and consequently in the discussion of the results. The equilibrium phase β (Mg_2Si) does not form below 200 °C and has not been observed in any of the analyzed specimens.

II. EXPERIMENTAL

Six pure Al-Mg-Si alloys were prepared with compositions given in Table II. Each alloy batch weighed 4 kg. After casting, they were homogenized 2 hours at 570 °C and extruded into the shape of thin bars having a rectangular cross section (25 × 2 mm^2). The bars were cut into samples of dimensions 25 × 25 × 2 mm^3. The heat treatment consisted of solution treatment 2 hours at 570 °C, water quenching at RT, 4 hours storage at RT, and a final aging at 175 °C. Aging time varied between 30 minutes and 208 hours. All samples are labeled using two numbers: Ax/xxh. The first number refers to the alloy type; the second gives the aging time in hours (h).

Vickers hardness measurements (1-kg load, 10 indentations per sample) were performed for each sample using a Matsuzawa DVK–1S unit (Akashi, Corp., Japan). Based on the hardness curves, different samples were selected for TEM specimens (Table III).

The TEM specimens were prepared by electropolishing using a Tenupol 3 machine (Struers, Denmark). The electrolyte consisted of 1/3 HNO_3 in methanol and the solution was kept at a temperature between −20 °C and −35 °C. A PHILIPS*

---

*PHILIPS is a trademark of Philips Electronic Instruments Corp., Mahwah, NJ.

CM30T, operated at 150 kV, was used for conventional TEM work, such as images for the number density counts. This instrument is equipped with a Gatan parallel electron energy loss spectrometer (EELS) (Gatan, UK). The EELS was used to determine specimen thickness of the area in the center of a micrograph.

Table II. Composition of the Investigated Alloys

Alloy Composition/ (Si + Mg) Designation At. Pct	Solute Content		Total	Solute
		Ratio Wt Pct (Si/Mg)		At. Pct
A1	1.1Si 0.2Mg	1.057Si 0.222Mg	1.28	4.76
A2	0.88Si 0.36Mg	0.8456Si 0.4Mg	1.24	2.115
A3	0.75Si 0.52Mg	0.721Si 0.577Mg	1.3	1.25
A13	0.41Si 0.28Mg	0.39Si 0.31Mg	0.7	1.26
A12	0.59Si 0.65Mg	0.57Si 0.72Mg	1.29	0.8
A11	0.45Si 0.78Mg	0.43Si 0.86Mg	1.29	0.5

Table III. Selected Aging Times at 175 °C, for Investigated TEM Specimens

Aging Time at 175 °C/Alloy	3 h	17 h	36 h	208 h
A1	*	—	*	*
A2	*	—	*	*
A3	*	*	*	*
A13	*	*	—	—
A12	*	*	*	*
A11	*	*	*	—

The TEM pictures at different magnifications were recorded on film for measuring particle volume densities (160 k), average needle lengths (89 to 160 k), and average cross sections (160 to 600 k). All the TEM analyses were performed with the Al matrix in a <100> zone axis. The needles usually cross the specimen, and in this direction, there is no aluminum below or above a precipitate.

For particle density measurements, the particles were counted visually from the TEM negatives. Only needles in the zone axis direction were counted (the dark spots in the <100> direction normal to the paper plane). To reduce the effect of nonuniform particle distribution, about ten bright-field images from different grains were analyzed for each of the specimens. A suitable magnification allows 100 to 400 precipitates to be counted from each negative. The thickness is measured for each negative, using EELS. This is necessary for quantifying the number densities and the according volume fraction of the precipitates for each micrograph. The

number density is defined as $\rho = 3 \, N/V = 3 \, N/At$, where the number of precipitates (N) is measured over a volume V (μm^3). The term A is the area on the micrograph where precipitates are counted for a specific specimen thickness (t), as measured at the center of this area. The factor 3 arises because only needles along one of the $<100>$ directions are counted. For number densities, it is necessary to correct for the fraction of needles included having centers falling outside the specimen; *i.e.*, needles can be considered to have been counted from a thickness that is larger than the specimen thickness. For this, the average needle length (λ) is needed. The effective thickness will be $t + \lambda$, so that the expression for number density as measured for one TEM micrograph becomes

$$\rho = \frac{3N}{A(t + \lambda)}$$

The standard deviation of ρ usually lies between 0.1 and 0.15 and is dominated by that of thickness $\sim$0.09. For ten or more images, the error in the average number density will be on the order of 5 pct (0.05). For each specimen, the average length of 400 to 500 needles and the cross sections of 50 to 100 particles are measured. The precipitate volume fraction is obtained by multiplying the particle number density with the average needle length and the average cross section. The maximum *error* in the estimated average volume fraction is usually less than 0.3 when 10 to 15 images have been used.

In the current experiments, the specimens for the Mg-rich alloys are the most difficult to study. A surface layer is found to occur that sometimes degrades the image quality. The measurements on the Si-rich alloys are therefore more accurate.

Explanation of the particle quantification method can be found in more detail elsewhere.[10] In Reference 10, a spot contamination method was used to determine the thickness of the samples. The introduction of EELS to measure sample thickness has simplified and improved this type of quantification significantly. Examples of the use and validity of the method can be found in References 9 and 11. In Myhr *et al.*,[11] the quantified number densities/volume fractions of the precipitates were used to model the age hardening behavior of the Al-Mg-Si alloys, with good results. Donnadieu[14] provides for additional comments on quantitative determination of number densities and volume fraction in an Al-Mg-Si alloy.

The precipitate volume fraction gives some information about the amount of solute consumed by the precipitates: one unit cell of β'' ($Si_{12}Mg_{10}$) equals the volume taken by 24 Al atoms. Alloy A3 (Table II) is optimized for β''. The amount of solute is 1.3 at. pct. If precipitates consume all the solute, the volume fraction is approximately (24/22) $\times$ 1.3 = 1.42. If the alloy were optimized for β', a maximum fraction would be $\sim$1.51. A maximum volume fraction of GP zones would be near 1.3. U1 and U2 would give $\sim$1.42 and 1.50. Most investigated alloys contain β'' in large proportions. Therefore, measured volume fractions can be compared to the maximum according to that of β''. The Si plates were not quantified and $\beta Mg_2 S_i$ has not been detected in the current work.

For the phase identification work, up to 40 particles per specimen were analyzed from HR images for the alloys A1,

A2, and A3 and up to 50 nanodiffraction patterns per specimen for alloys A11 and A12. A PHILIPS CM30UT/FEG electron microscope, operated at 300 kV, was used for all HR work. Its point-to-point resolution of 0.17 nm is well suited to determine the precipitate type when the periodicity is visible. Experience has shown that precipitate phase determination by HREM in the Al-Mg-Si system is relatively easy, but time-consuming. When using HREM images, the number of particles in one image is usually below five, and obtaining statistics becomes tedious work. Figure 1 gives representative HR images and diffraction patterns in the cross section from the precipitates mentioned in this work. The particles must be determined in cross section; otherwise, the needle would be embedded in the aluminum matrix. With experience and knowledge of the different precipitate unit cells, unless a particle is disordered or heavily distorted, *e.g.*, by strain, from HREM images of the $<100>$ Al projection, it is possible to recognize the precipitate type by analyzing its periodicity. The projected *unit cell* size and shape is unique. If necessary, the structures can be verified by fast Fourier transforms (FFTs) of areas of the particle cross sections of the HREM images. (e.g., Figure 1(b)). An FFT of the image of a disordered particle often reveals diffraction spots that can be related to a phase.

Alternatively, one can determine the particle type using nanodiffraction. However, this method is usually impractical for statistical analysis of the very small particles, such as GP zones, mainly because of specimen drift, beam damage, and the longer time such analysis takes. A few examples of nanodiffraction from the current precipitates are shown in Figure 1.

Examples of phase identifications in the 6xxx alloy system can be found elsewhere.[5,6,10,12,14,15]

IV. RESULTS

A. *Si-Rich Alloys*

The total Mg + Si amount in the three Si-rich alloys A1, A2, and A3 was kept at 1.3 at. pct (Table II). The A1 and A2 have Si/Mg ratios of 4.7 and 2, while A3 has a ratio of 1.25. Therefore, the solute ratio of A3 corresponds to a ratio near that in β'' (Mg_5Si_6). In this way, one can observe how the precipitate microstructure changes with increasing Si content relative to an alloy "optimized" for β''. Important for the comparison is the fact that quenched-in vacancy concentration should be similar in all the alloys, since they undergo the same heat treatment.

1. *Hardness curves*
The hardness curves for the isothermal heat treatments at 175 °C are presented in Figure 2(a). It can be seen that all the curves display similar profiles: the hardness increases rapidly to a sharp maximum after 3 hours of aging. After a small decrease, hardness builds up to a second, broad maximum that lasts 30 to 40 hours. Upon further heating, the material "overage" and the curves display a continuous decline. As expected, the alloy optimized for β'' (A3) is the strongest while the most Si-rich alloy (A1) is the weakest. At peak hardness, A3 reaches the same value ($\sim$96 HV) for both the sharp and broad peaks. A fourth Si-rich alloy (A13), similar to A3 but with lower alloy content, displays a different type of behavior and is discussed in Section C.
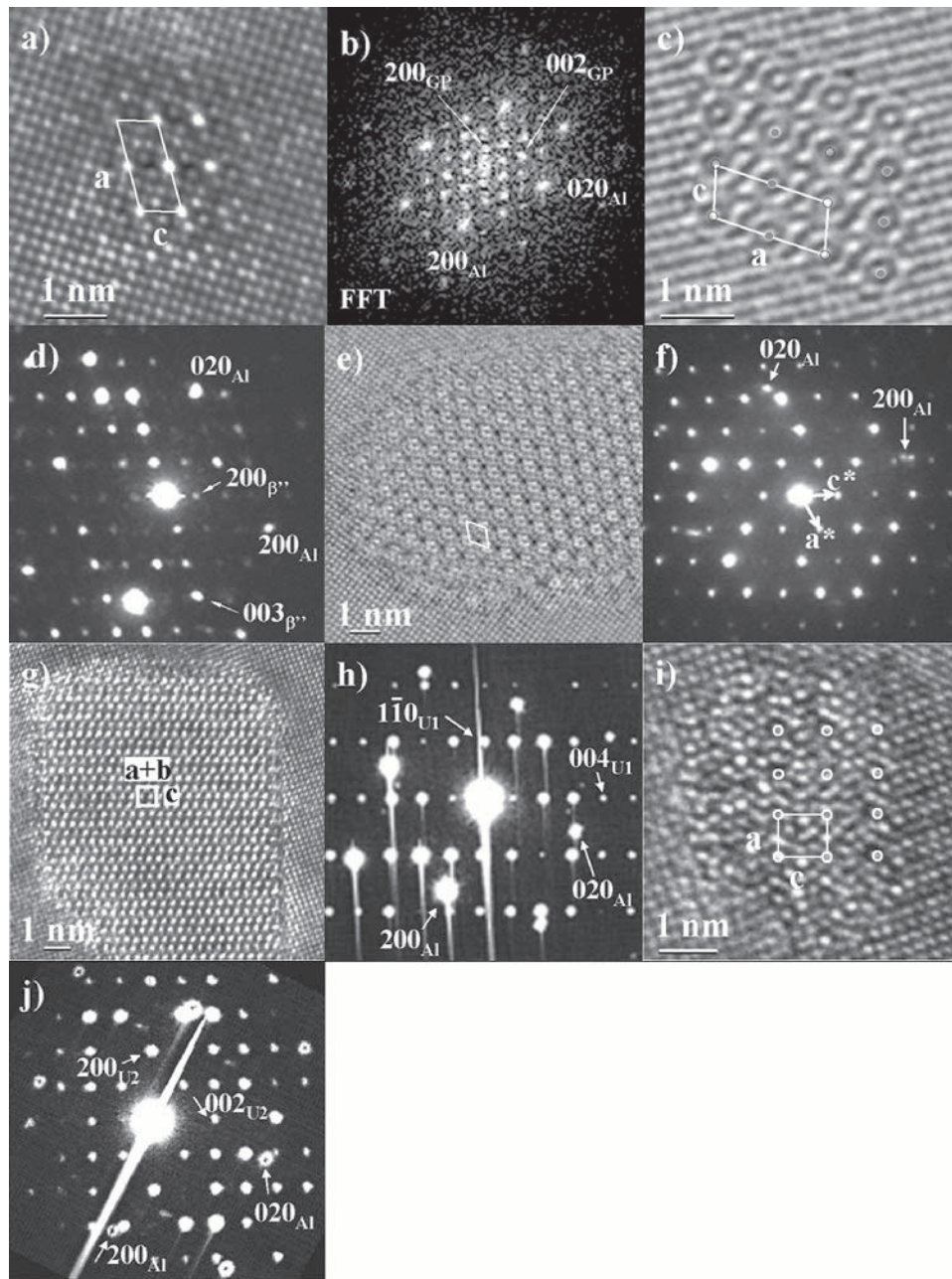
Fig. 1—Phase determination using high resolution (HR) and nanodiffraction (ND): (*a*) "perfect" GP zone, (*b*) FFT of (*a*), (*c*) HR image of perfect β'', (*d*) ND of β'', (*e*) HR of β' precipitate, (*f*) ND of β', (*g*) HR of U1 precipitate, (*h*) ND from a U1-phase, (*i*) HR of U2 precipitate, and (*j*) ND of U2. All precipitates are easily identifiable in both imaging and diffraction modes. ND could not be performed on the GP zones due to their small size. The streaks observed in some of the patterns are due to oversaturation in the CCD camera.

2. *Particle sizes and densities in Si-rich alloys*

The results from the TEM analysis of the selected samples (Table III) are shown in Figure 3. The main conclusions are as follows.

(a) Particle density is reduced with time as precipitates coarsen.
(b) For 3 hours annealing, for higher Si content, more particles were detected, but after 36 hours, the number density was more similar for all the alloys.
(c) The precipitates coarsen with time, but between 3 and 36 hours, cross section and needle length increase only

a little. This corresponds to the broad maximum "plateau" in the hardness curves.
(d) The particle cross sections and—to a lesser extent—the needle lengths decrease with increasing amount of Si.
(e) The volume fraction decreases with increasing Si/Mg ratio. Even for the alloy with the highest hardness (A3), the estimated particle volume fraction is low; for A1 to A3, at most, 10 to 50 pct of the alloying content is used for precipitation. The shorter the annealing time the lower the yield.

Examples of the precipitate microstructure for the Si-rich materials A1/36h, A2/36h, and A3/36h are shown in
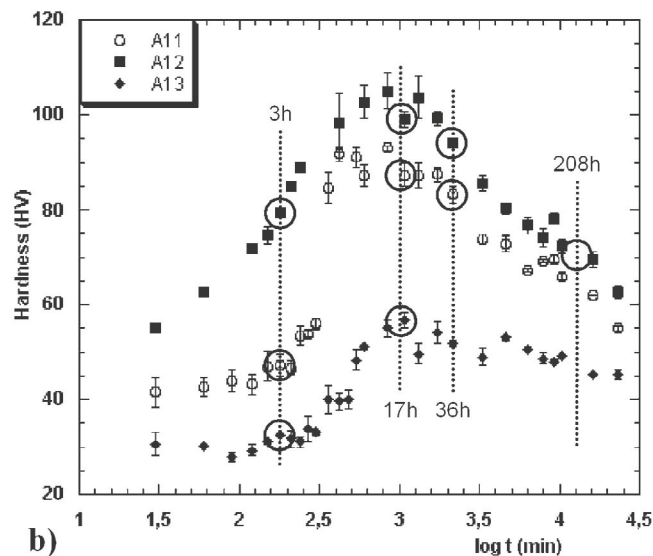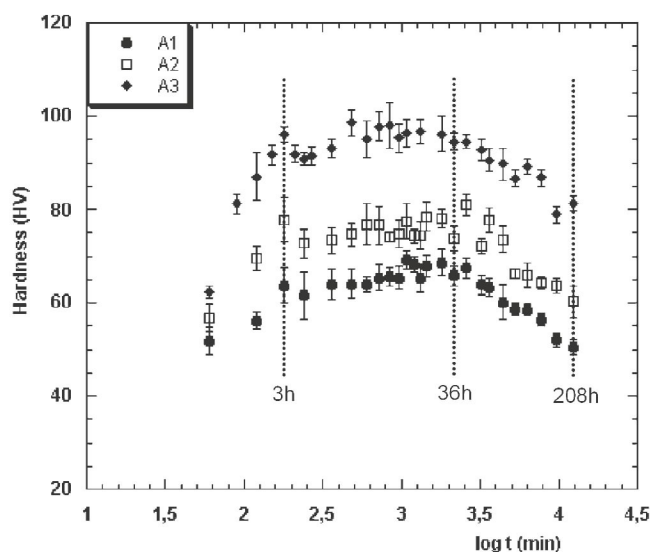
Fig. 2—Hardness curves for all alloys as a function of aging time at 175 °C. Alloys contain 1.3 at. pct Si + Mg except A13. (*a*) Si-rich side: Hardness increases with decreasing Si until Si/Mg = 6/5 (A3). Notice the GP zone peak after 3 h. (*b*) Mg-rich side: Hardness increases with decreasing Mg until Mg/Si = 6/5 (A12). The GP zone peak is not visible. The Si-rich alloy A13 (~A3 with half amount of solutes) behaves like Mg-rich alloys. Specimens selected for TEM investigation are indicated by circles. Alloy legend: Table II.

Figure 4. The figure illustrates a slight increase in the cross section of GP zones and β'' when decreasing the Si/Mg ratio in the alloy from (a) 4.8 to (c) 1.25, while the precipitate number density is more similar. Dark spots (needles viewed in cross section) and needles along the <100> directions are used for estimating the parameters shown in Figure 3. The double stripes around the precipitates seen edge-on originate from interface strain in both β'' and GP zones.

3. *HREM study of particle types in Si-rich alloys*

In order to find the approximate relative amount of various types of precipitates present in samples 5 through 10, HREM images from each specimen with the matrix in a <100> zone axis were recorded on film and were analyzed. The results are given in Table IV.

The conditions A1/3h and A2/3h were not investigated in HR, but a GP-zone microstructure can be assumed due to the similar hardness profile after 3 hours for all of the Si-rich alloys. Figure 5 gives examples of the precipitates found in these alloys. In the figure, arrows have been superposed to clarify the lattice periodicity (*cf.* with Figure 1). The figure illustrates that for higher Si content, GP zones become stable for long-time aging (a). In the optimized alloy A3 (Figure 6) with Si/Mg ~1.2, the β'' phase is stabilized and well ordered and only small fractions of other phases occur. Increased Si/Mg ratios are seen to cause a higher fraction of intergrown β''/U2 (Figure 5(b)) and β'/U2 (Figure 5(c)), as well as disordered β'' and more β'. For the highest Si content (Figure 5(d)), Si plates form. Sometimes these plates are also intergrown with other phases. Figure 5(d) shows a Si crystal in a <110>-type zone. The {111} lattice planes (d = 0.313 nm) are indicated by parallel lines. This Si <110> zone axis is parallel with <001> zones in both Al and β'. Figure 5(e) also shows a disordered GP zone (A1/36h). To determine this solely from the HREM image is not trivial. The atoms are nearly on the Al positions. However, when subjected to an FFT, the disordered region seen in the matrix gives clear indication of the monoclinic GP/β'' unit cell (f) (*cf.* with the ordered GP zones in Figure 5(a) and Figures 1(a) and (b)). The parallel stippled lines in Figure 5(f) are recognized as the <10 *n*> rows of the GP zones (or β'') that are directed along Al <301> directions. The following conclusions can be drawn.

(a) After 3 hours of aging, culminating in the first hardness maximum, the matrix contains a high number density of fully coherent GP zones. The first peak is therefore the signature for the GP zones.[15]

(b) The second, broader maximum (17 to 36 hours) is caused by fewer but coarser particles, mainly of the β'' type for the strongest alloy (A3) (Figure 6, A3/17 h). The number of GP zones counted increases with increasing amount of Si. The alloys of high Si content, A1 and A2, contain particles with a more disordered atomic arrangement in the needle cross section (001 plane). They are more likely GP zones than β'', and must be the reason for the smaller cross section observed with the higher Si content.

(c) Even after 208 hours, the picture is similar. In A3, the main phase is β''. Very little has transformed to β' or other phases. For the highest Si content (A1), a considerable fraction of GP zones survives. Large amounts of β', U2 phase, and Si plates are found in A1 and A2 (Figures 5(b) through (d)). The number of precipitates of type U2 exceeds greatly that of U1. Only one of 23 particles was found to be of the U1 type in A1, and no U1 precipitates are found in material A2. In short, an increase in Si content gives less β'' but more GP zones, disordered β'', β', Si plates, and U2 phases.

(d) Many particles in the Si-rich A1 and A2 alloys are found to be a mixture of β'', β', and U2 crystals (Figure 5(b) and (c)).
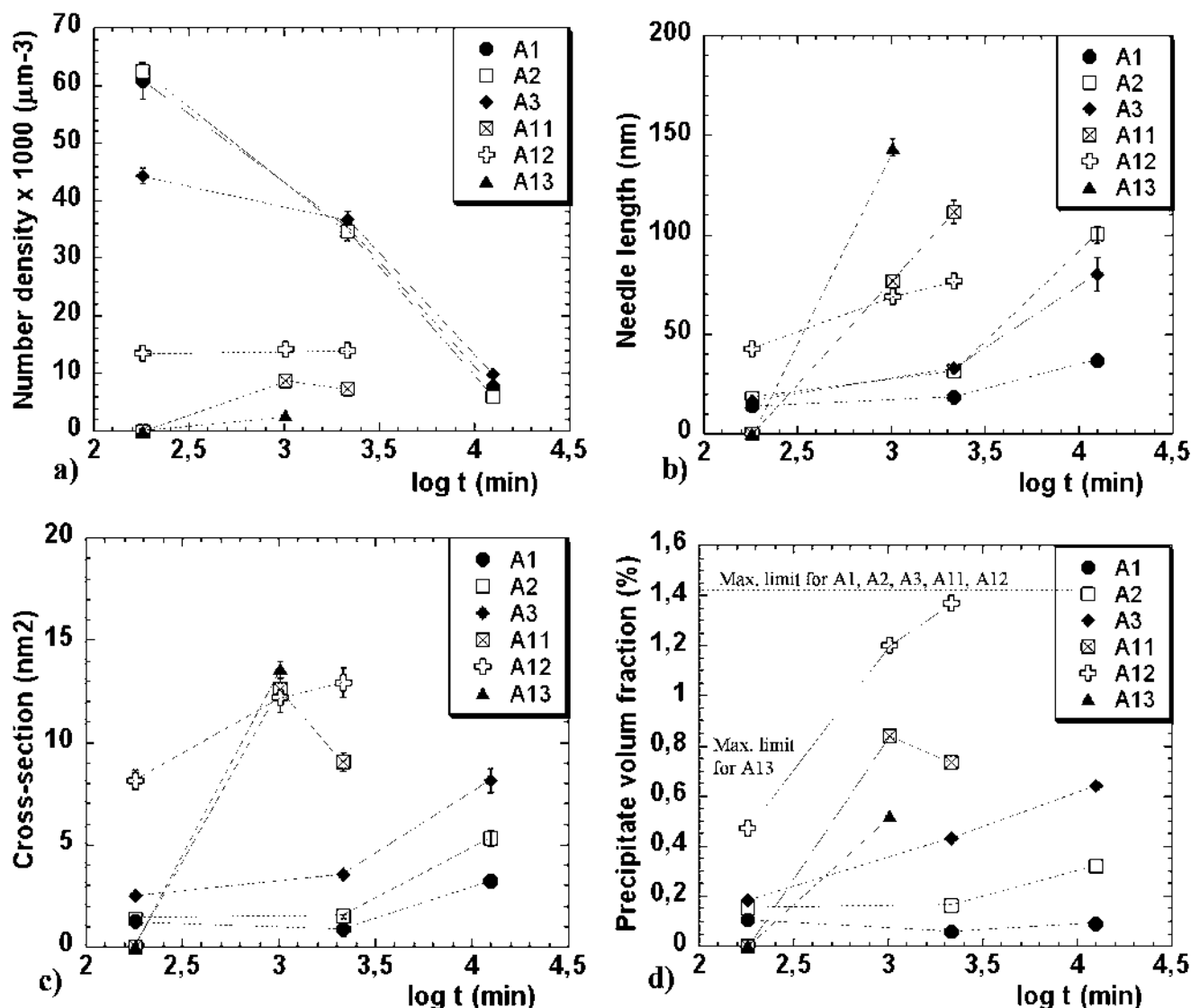
Fig. 3—Quantitative TEM measurements of the precipitates for all six alloys as a function of artificial aging time: Estimates of (*a*) average precipitate number density (number/μm^3), (*b*) average length of precipitate needles, (*c*) average cross section, and (*d*) volume fraction. Maximum limit—approximate volume fraction if all solute atoms enter into precipitates. In Si-rich alloys, much more solute remains in solution or as undetectable clusters as compared to that in Mg-rich alloys. Alloy legend: Table II.

B. *Mg-Rich Alloys*

1. *Hardness curves*

The investigation comprised two Mg-rich alloys—A11 and A12—having the same total amount of solutes as the Si-rich alloys: Mg + Si = 1.3 at. pct. The relative amount (Mg/Si) was 2 for A11 and 1.25 for A12 (Table II). Note that A13, the Si-rich alloy with 0.7 at. pct solutes, is included in the hardness curves of Figure 2(b), since it displays similarities to the Mg-rich alloys. The hardness response of the Mg-rich alloys differs strongly from the Si-rich alloys. For short aging times, the smaller Si/Mg ratio suppresses the first hardness peak (Figure 2(b)). This effect is most pronounced for A11 having the lowest ratio. The hardness curves therefore mainly display a single maximum, approximately after 17 hours of aging. The subsequent fall in hardness is quicker on the Mg side, which means these alloys overage faster. However, the maximum

hardness is similar to or even higher than for the Si-rich alloys (105 HV for A12 *vs* 96 HV for A3 after 17 hours aging). A12 is stronger than A11, but they differ with less than A2 and A3 (Figure 2).

2. *Particle sizes and densities in Mg-rich alloys*

The TEM analysis of the Mg-rich alloys leads to the following conclusions (Figure 3).

(a) After 3 hours, only little precipitation has taken place in A12. In the most Mg-rich alloy, A11, no precipitation at all can be observed. This corresponds to the initial region of low hardness in Figure 2(b).

(b At peak hardness (17 to 36 hours annealing), the precipitate microstructures of A11 and A12 are much coarser than of the Si-rich alloys.

(c) In general, the particle number density is 4 to 7 times lower than for the Si-rich alloys. Precipitates of the most
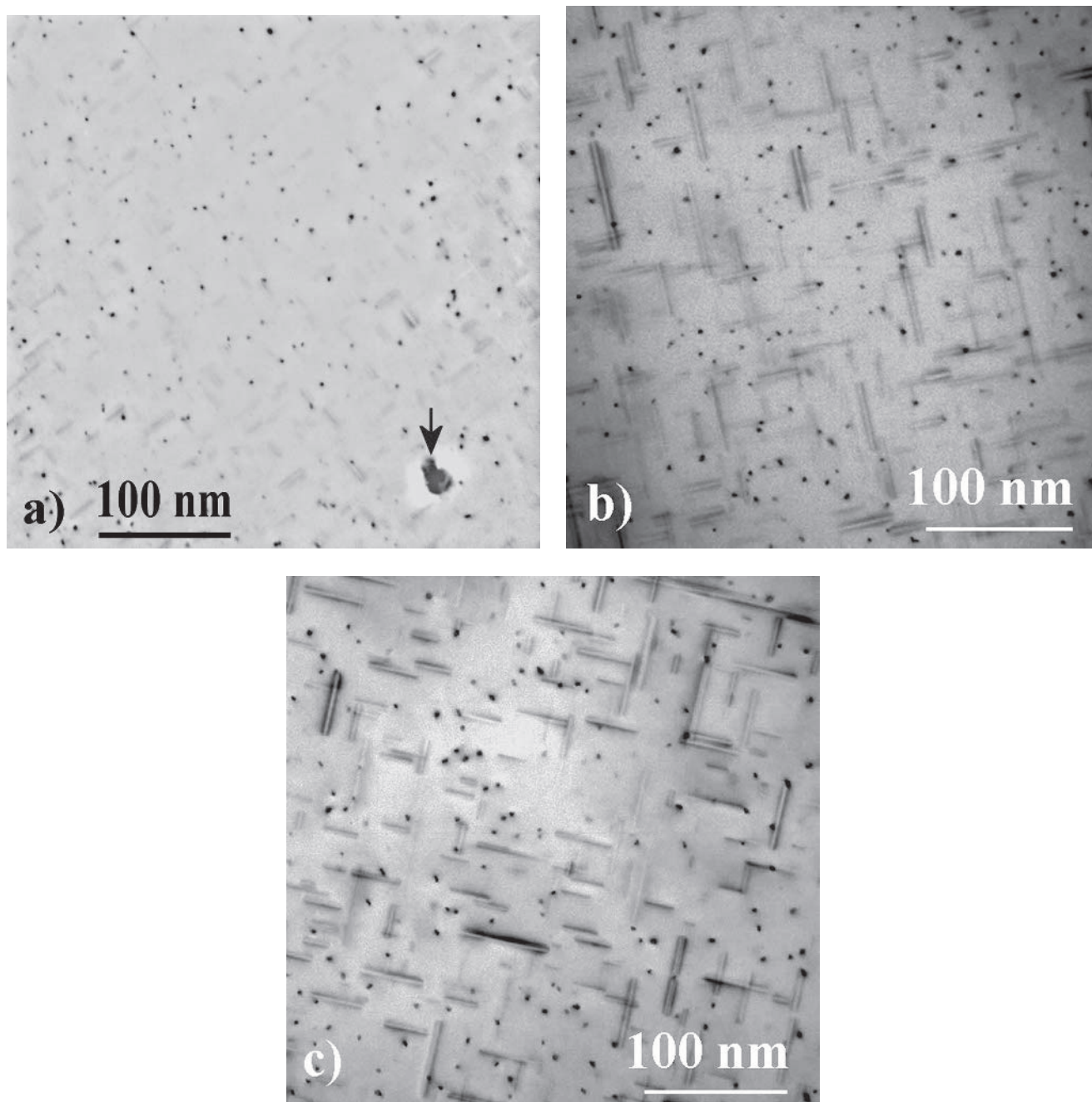
Fig. 4—TEM bright-field images of the Al <001> zone showing a slight increase in precipitate cross section of GP zones and β'' when decreasing the Si/Mg ratio from (a) 4.8 for A1/36h through (b) 2.1 in A2/36h to (c) 1.25 in A3/36h. Arrow (a) shows the Si plate in A1 coexisting with GP zones and β''.

Mg-rich alloy, A11, coarsen fastest and A11 was found to contain the least particles.

(d) The volume fraction of precipitate particles is significantly higher than in Si-rich alloys. A12 has a higher volume fraction than A11.

In Figure 7, the specimens A3/3h (optimized alloy) and A12/3h are compared, having Si/Mg ratios 6/5 and 5/6, respectively. This figure visualizes some of the preceding observations, *i.e.*, that the Mg-rich alloy coarsens faster. Precipitates showing the double-line contrasts are either GP zones or β''. In Figure 7(b), one can also see precipitates with narrow rectangular cross sections heterogeneously

nucleated on a dislocation line. They are possibly B$'$.[5] The relatively small cross section measured in alloy A11 after 36 hours aging causes the volume fraction to drop. The reason for this is uncertain. It is possibly an error in the cross-section measurements or due to inhomogeneous particle size distribution.

3. *HREM study of particle types in Mg-rich alloys*

The lower amount of precipitates in the Mg-rich alloys made the HREM imaging technique less useful for quantification of the different types of precipitates. Therefore, in addition to HREM images, *nanodiffraction* was used, where a finely focused electron beam placed on a precipitate

Table IV. Relative Frequency of Various Types of Precipitates as Observed by HREM/Diffraction after 3, 36, and 208 Hours of Aging*

Particle Type/Sample	GP Zones (Pct)	Disordered (Pct)	β'' Phase (Pct)	β'/U/Si Plates (Pct)	Number Analyzed
A3/3h	86 ←	14	—	—	35
A12/3h	— ←	78	→ 22	—	9
A1/36h	22 ←	44	→ 4	31	23
A2/36h	4 ←	34	→ 59	4	24
A3/36h	—	32	→ 69	—	38
A12/36h	—	22	→ 66	→ 12	59
A11/36h	—	74	→ 22	→ 4	50
A1/208h	13 ←	26	→ 9	52	23
A2/208h	—	10	→ 53	38	21
A3/208h	—	19	→ 77	4	26
A12/208h	—	28	→ 31	→ 41	29

*Up to 59 arbitrarily chosen particles were analyzed per condition. For some conditions, the total precipitate percentage is 101 pct due to the numerical rounding of the data. The β'' is most numerous for Si/Mg near one (A3, A12). When Si/Mg ~6/5 (A3), most perfect β'' particles form. High Si content stabilizes GP zones (A1/208h). Arrows give possible classification of disordered precipitates. The β', Si plates, and U phases are grouped together. The Si plates are only found in A1 and A2. After long annealing times, more U2 and β' are found in A1 and A2. Most particles in Mg-rich alloys in this classification are β'.

gives rise to diffraction. The results of this investigation are given in Table IV. In Figure 8, a few examples are given of the precipitates found in the Mg-rich alloys (all pictures are taken from specimen A12/36h). When the Mg/Si ratio increases from 5/6, a significant fraction of both (a) and (b) β'' and (c) and (d) β' phases clearly becomes disordered. For examples of perfect precipitates, see Figure 1. In Figure 8(a), a unit cell is superposed on a disordered β'' precipitate. The β'' nature of this precipitate becomes clearer in the FFT image (Figure 8(b)). There are additional reflections in the FFT image that could not be identified. Figure 8(c) shows a disordered β' precipitate. The FFT (d) reveals a ring of six equally arranged weak reflections (stippled circles) indicating that hexagonal β' is present in part of this precipitate. This FFT also contains unidentified reflections. The nanodiffraction patterns in Figures 8(e) and (f) are from a perfect and a disordered β'' precipitate, respectively. The conclusions from the Mg-rich alloys are as follows.

(a) After 3 hours of aging, the microstructure of the least Mg-rich alloy, A12, consists mainly of disordered β'' needles.
(b) At peak hardness, the microstructure of both A11 and A12 is mainly a mixture of β'' and β', but a high fraction of the particles have an atomic arrangement with a disordered appearance. By using FFT, the type of the precipitate can be determined. Also, the disorder in these precipitates is "visible" in nanodiffraction patterns (Figures 8(e) and (f)).
(c) As opposed to the Si-rich alloys, the amount of precipitates of the U2 type is very low. Only one particle of 59 analyzed was of type U2 in A12/36h and one of 29 analyzed in A12/208h. No particle of type U2 was observed in A11/36h, where 50 particles were analyzed.
(d) In general, the higher the amount of Mg in the alloy, the less β'' is found and more β' and disordered precipitates are observed. Neither GP zones nor any U1 particles have been observed in any of the samples.

C. *Alloy A13*

A particular situation occurs for alloy A13. Just as A3, this alloy is Si rich with a Si/Mg ratio equal to 1.2, but it contains half the level of solutes—a total of 0.7 at. pct (Table II). As expected, due to the lower amount of solutes, A13 displays a much lower hardness than the rest of the alloys (Figure 2(b)). It was also expected that the profile of the hardness curve would be similar to the other Si-rich alloys. As seen in Figure 2, the curve instead shares a high similarity with the Mg-rich alloys. The TEM analysis gave further evidence of this. Just as for the Mg-rich alloys, no precipitation is visible in the specimens aged 3 hours. Also, a coarse microstructure resembling that found in Mg-rich forms in the peak hardness condition (Figure 3) with a high precipitation volume fraction as compared to the total amount of solutes (0.5 pct *vs* 0.76 pct). Such high volume fractions are also characteristic for Mg-rich alloys, as shown previously.

V. DISCUSSION

The aging response of the Si-rich alloys differs clearly from that of Mg-rich alloys (Figure 2). Hardness is low for both high and low Si/Mg ratios in the alloy. When the ratio approaches one, from both sides, a high hardness is achieved, but the width of the hardness peak is considerably smaller on the Mg side. On the Si side, a sharp initial peak develops after 3 hours. The HREM study connects this peak to a high density of very fine needle-shaped GP zones. After longer annealing time, a second, wide, hardness peak (plateau) follows, which extends from about 10 to 40 hours. In the Mg-rich alloys, the early peak is practically absent. Instead, the hardness response may be described as a single peak at about 20 hours. Although β' particles are also found, the single peak on the Mg-rich alloys is caused by coarser needles of mainly β'' phase as compared with the Si-rich alloys. Therefore, in Si-rich alloys, both GP zones and β'' are responsible for the strength, while in Mg-rich alloys, β'' is the most important precipitate.

It is helpful for the understanding of microstructure development to relate the results obtained at peak hardness to the early stages of precipitation. This involves atomic clusters that could nucleate subsequent phases in the precipitation sequence as GP zones and β''. Although such investigations
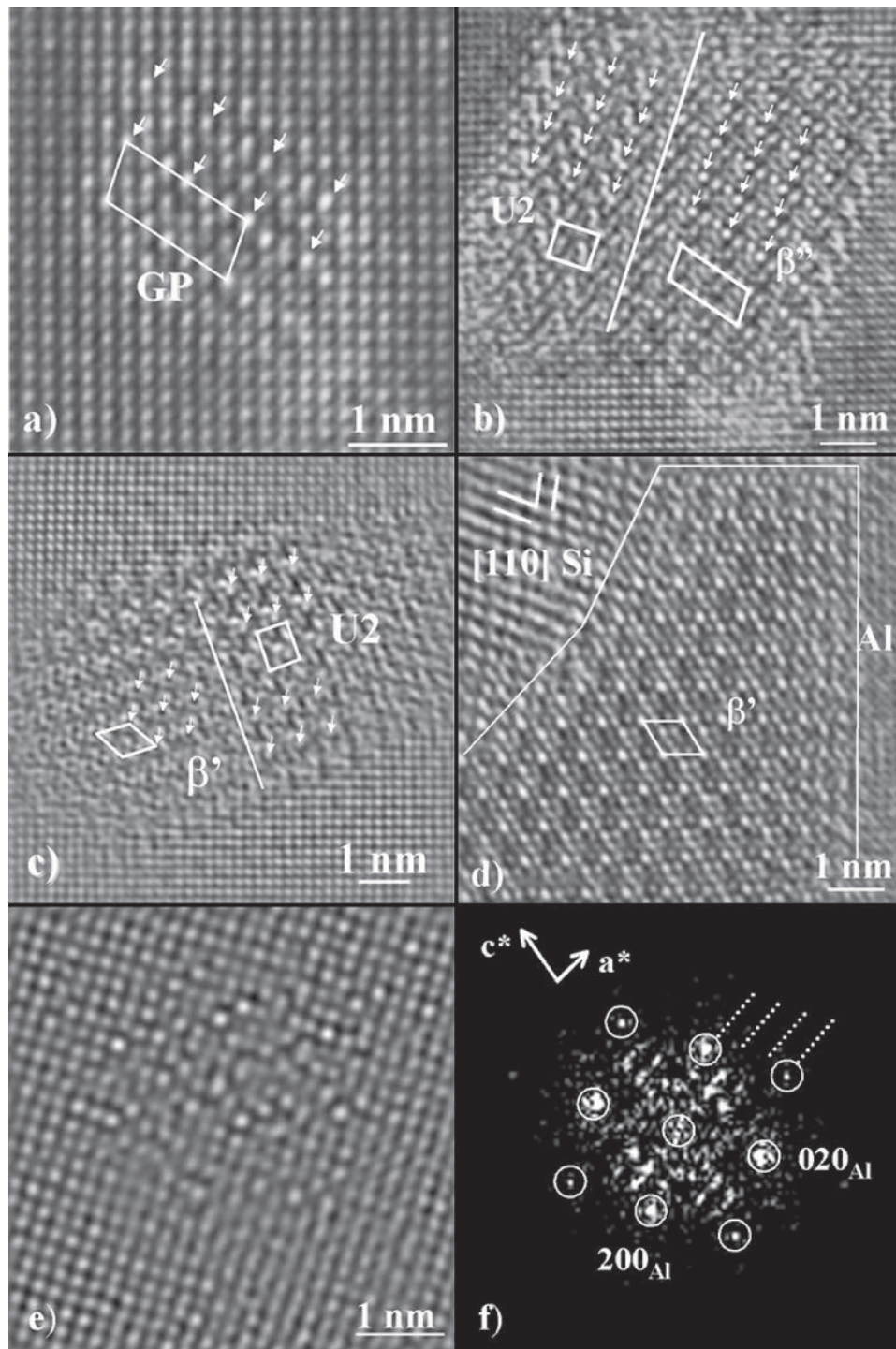
Fig. 5—Examples of precipitates in the Si-rich alloys. Arrows are superposed to clarify periodicity. (*a*) A2/36h: In alloys with Si/Mg ~2, GP zones become stable for longer aging times. (*b*) and (*c*) A2/208h: Prolonged aging gives a higher fraction of (*b*) β''/U2 and (*c*) β'/U2 intergrowth, disordered β'', and more β'. (*d*) A1/208h: As Si content is raised (Si/Mg = 4.8), more Si plates form and intergrow with other phases. (*e*) Slightly disordered region in the matrix (A1/36h). (*f*) The FFT image identifies it as the GP zone.

have not been part of the present work, important information exists in recent publications[2,3,4] involving atom probe field ion microscopy. It has been found that the as-quenched condition, just after solution heat treatment, contains separate Si and Mg clusters. The prevailing supersaturated solid solution, together with a high vacancy concentration, allows additional Si-Mg co-clusters to develop at low temperatures.[2,3,4] However, if the material is annealed at temperatures above 70 °C, the Mg clusters seem to dissolve and the Mg atoms migrate to the pre-existing Si clusters.[2] The formation of clusters from solid solution at RT is a process that can be observed indirectly by the slow increase in hardness that can go on for months in Al-Mg-Si alloys. It has also been shown that Si-rich clusters are vacancy traps.[16]
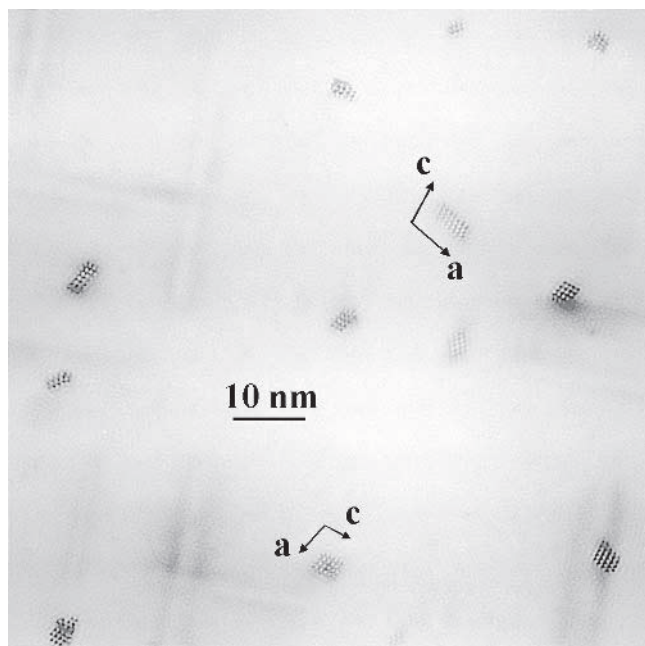
Fig. 6—In the optimized material for β'', precipitates are ordered, and even for lower resolution images, they can easily be determined to be β''. They are homogeneously distributed, with cross sections having the monoclinic angle, allowing the number of unit cells in the a-c plane to be counted. The image was taken from condition A3/17h using the CM30 conventional instrument (point to point resolution 0.23 nm). The image can be seen as a higher magnification of Fig. 4(c). Unit cell directions are shown for two of the precipitate cross sections. For presentation purposes, lower spatial frequencies of the image have been suppressed by FFT filtering.

This means that the growth of clusters in general will be slower in alloys when increasing the amount of Si because of limited diffusion. One can expect the lower amount of vacancies available also to influence the hardening phases. In general, for the alloys presently investigated, this means that the higher the Si/Mg ratio is in the alloy the more Si-Mg co-clusters should form. If the co-clusters provide nucleation sites for the subsequent precipitates, then the precipitate number density is expected to be high in the Si-rich alloys. Figure 3(a) confirms a high particle number density in alloys A1, A2, and A3. Also, since a high amount of Si-rich clusters reduces diffusion, the microstructure in the Si-rich alloys should be fine, with low volume fraction. This is supported by the observation that in Si-rich alloys, the overall precipitate volume fraction is low. Even if a higher Si/Mg ratio causes more precipitates to develop, they will be finer and therefore yield lower precipitation volume fractions (Figure 3(d)).

The high Si content in alloys A1, A2, and A3 favors the formation of a large number of fine GP zones after short annealing time. The strain field introduced in the matrix by their growth causes the hardness to increase and a maximum is reached after 3 hours aging. The GP zone number density increases with the Si amount, but its size is reduced and the particles become less efficient in pinning dislocation movement. Alloy A3 is therefore the strongest, while the most Si-rich A1 has the lowest hardness. For longer annealing time, some of the GP zones dissolve while others transform to β'' phase,[15] and a broad, second hardness peak develops, centered at about 20 hours. The width
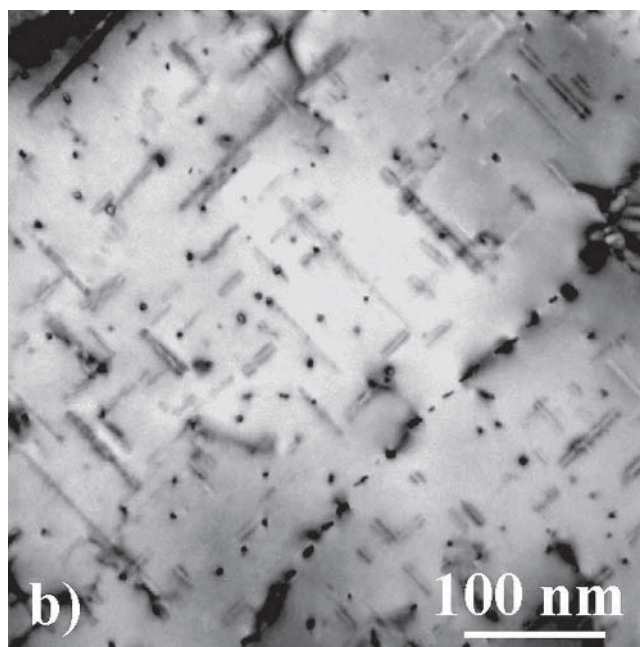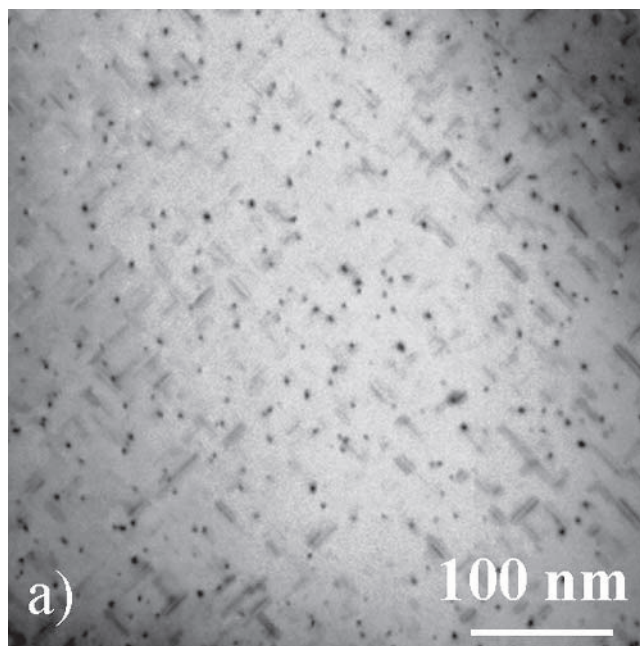

Fig. 7—Comparison between (*a*) Si-rich (A3/3h) and (*b*) Mg-rich (A12/3h) alloys with Mg/Si ratios 5/6 and 6/5, respectively. The Mg-rich alloys have fewer and coarser precipitates yielding higher volume fractions. (a) HREM showing precipitates that are mainly GP zones. (b) Precipitates are more complex. A large proportion of the precipitates are disordered, while about 20 pct are pure β'' (the shortest needles with double-line contrasts). (b) The precipitates with narrow rectangular cross sections nucleated along the dislocation line are probably of B$'$ type.

of the peak is related to the good stability of the β'' precipitates at the temperature of the heat treatment (175 °C). Alloy A3 is the strongest because its composition favors the formation of β'', and this precipitate survives a long annealing time. An increase in Si content in alloys A2 and A1 causes the β'' needles to become more disordered, concurrent with the presence of a higher number of Si-rich GP zones and the formation of U/β' phases. The particle num-
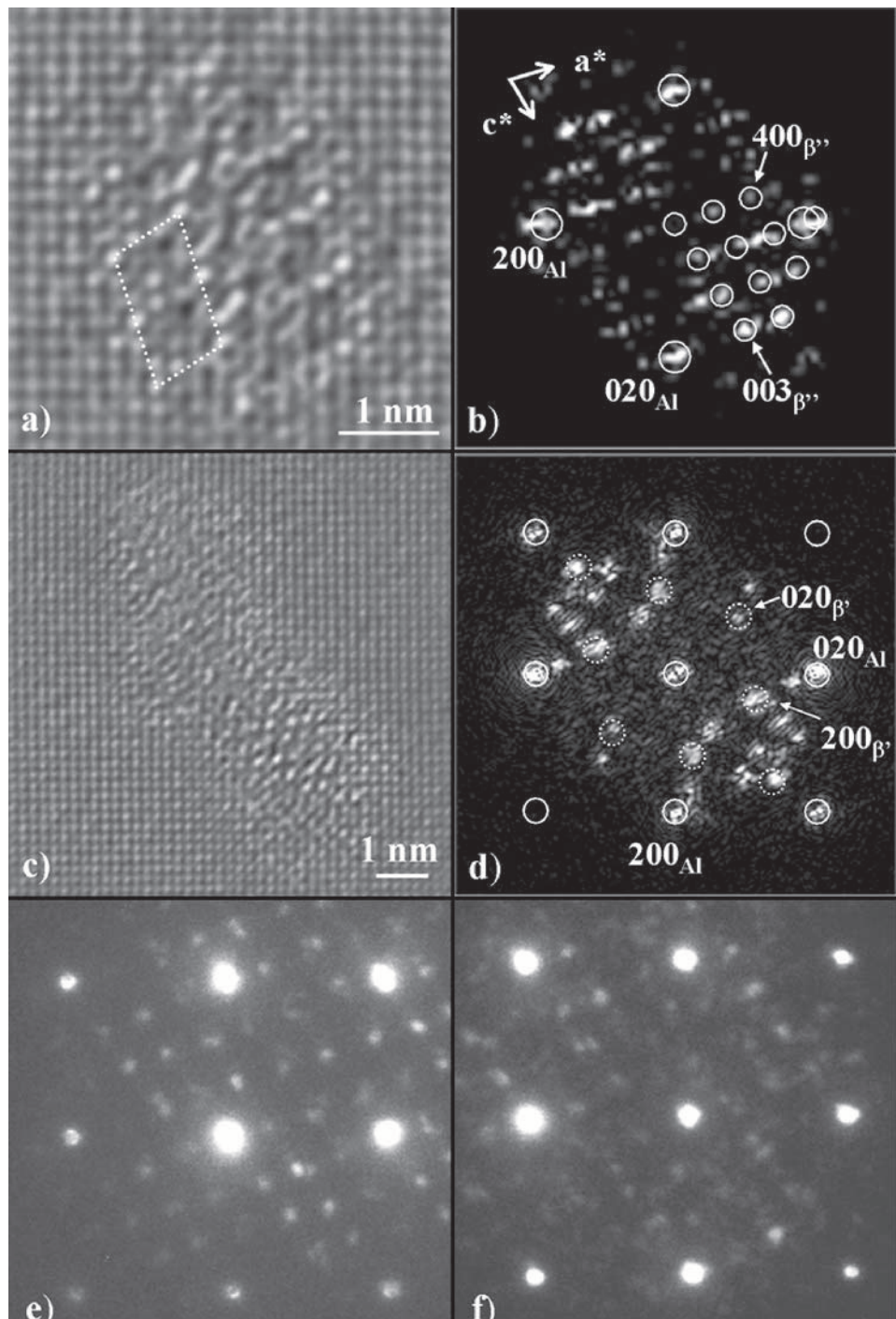
Fig. 8—Examples of the precipitates found in Mg-rich alloys: (*a*) disordered β'' precipitate of A12/36h with superposed unit cell, (*b*) FFT of (a) proving it is β'' and unidentified reflections, (*c*) Disordered β' precipitate from specimen A12/36h, (*d*) FFT of (c) where hexagonal β' structure becomes visible among unidentified reflections. (*e*) Nanodiffraction pattern from a perfect β' precipitate. (*f*) Nanodiffraction pattern from a disordered β''. For (e) and (f), the indexing is identical to (b). All pictures are taken from specimen A12/36h.

ber density is similar for the three alloys in the peak condition, but the overall particle size decreases with the increasing Si amount in the alloys' composition. As explained previously, this could be the result of low diffusion due to vacancy reduction by the Si-rich atomic clusters and GP zones. The effect of a small particle size is a decrease in the volume fraction and consequently in hardness for the most Si-rich A2 and A1.

With decreasing Si/Mg ratios, fewer GP zones reach a critical size that allows them to grow and influence hardness. The GP-zone peak is strongly suppressed in material A12 (Si/Mg = 5/6). When the Mg/Si ratio is increased to a factor 2 in A11, the GP-zone peak is absent. More Mg and vacancies are present and GP zones dissolve or nucleate/transform more easily to β''. The low amount of Si in A11 and A12 decreases the particle number density in these

alloys (Figure 3(a)). For the alloy with the most Mg, no precipitation was seen after 3 hours. As fewer vacancies are used for nucleation, more vacancies would be available for particle growth. The result is a coarse microstructure that overages faster. The peak hardness becomes comparable to or higher than the Si-rich alloys because the coarser β'' precipitates produce a high volume fraction; for A12, it was measured to be near the maximum achievable if all solute were incorporated in the particles. Alloy A12 is strongest because its composition is closer to the ideal composition of the β'' phase (Mg_5Si_6) and a larger fraction of the particles are of this type.

The behavior of A13, the alloy with the same Si/Mg ratio as A3, but with half the solute content, has an aging response that is more similar to the Mg-rich alloys because of the low Si content. Just as with A11, no precipitation could be seen after 3 hours, but the material goes through a subsequent rapid coarsening. At 17 hours, this material contains the largest precipitates, similar to the two Mg-rich alloys. The measured volume fraction is near the maximum attainable.

Figure 6 presents the precipitate microstructure for the alloy optimized for β'' after 17 hours aging. Practically all precipitates can be recognized as β''. A deviation from this solute ratio (Si/Mg = 6/5) is seen to cause a reduction in the number of β'' precipitates. The Mg- or Si-rich environment around the nucleation sites of many precipitates appears to lead to a disordered or "random" atomic arrangement, as seen in HREM images of the precipitate needle cross sections.[3] These precipitates are characterized by local "perfect" β'' (and to a lesser extent β'/U2 phases) atomic structures that may contain stacking faults. A detailed atomic description of one such fault has been discussed in an earlier publication.[12] For longer annealing times and for large deviations from the ideal composition, more U2/β'/Si plates are present in the Si-rich alloys. A common situation is β''/β'/U2 combinations in one needle. These precipitates intergrow because of similarities in their atomic structure.[7,17] The similar Mg/Si ratio or chemical composition of U2 (AlMgSi[7,8]) as compared to β'' and the structural relationships between these phases explain why the U2 phase is found in large amounts in the Si-rich alloys. Previous TEM studies indicate that in the early stages of nucleation and growth the GP zones are Si rich.[15] The present work confirms that GP zones survive for long aging times (at least 208 hours in A1) when increasing the Si content. More Si stabilizes GP zones against dissolution/transformation. This indicates that the Si/Mg ratio in GP zones is large and more similar to that of A1 ($\sim$5) than of A3 (6/5).

VI. CONCLUSIONS

1. The Si-rich alloys contain a very fine precipitate microstructure producing high hardness despite a low volume fraction of precipitates. The precipitates responsible for the strength are mainly GP zones and β'' having a near coherency with the matrix. The β'' phase is the most effective strengthening phase.
2. In the Si-rich alloys, after 3 hours aging at 175 °C, a sharp hardness peak exists that can be attributed to GP zones. This peak rests on a wider peak ($\sim$17 hours) corresponding to the β'' precipitates.
3. The hardness response of the Mg-rich alloys is a single peak coinciding with the center of the broad maximum in the Si alloys. The microstructure consists mainly of β'' and β', but β'' is responsible for strength.
4. The Mg-rich alloys have a coarse microstructure and overage faster than the Si-rich alloys.
5. If the alloy composition is changed from the ideal ratio Si/Mg = 6/5 the β'' precipitates display a more disordered atomic arrangement. An increasing number of other precipitates will also form.
6. The U2 is common in the Si-rich alloys for longer aging times. The U2 precipitate and a higher stability of β'' seem to be the main reasons for the slower overaging observed in the Si-rich alloys. Combinations of β''/β'/U2 in the same precipitate are observed.
7. The Mg-rich alloys contain less U phases, but are richer in β'.
8. A Si-rich alloy with a lower total content of solutes (A13) has a Mg-rich behavior. The precipitates are among the coarsest.
9. The results give a strong indication that Si controls the number of precipitates by clustering in the beginning of annealing.

REFERENCES

1. O. Reiso: Ph.D Thesis, Norwegian University of Science and Technology, Trondheim, 1992, pp. 1-19.
2. G.A. Eduards, K. Stiller, G.L. Dunlop, and M.J. Couper: *Acta Mater.*, 1998, vol. 46 (11), pp. 3893-3904.
3. K. Matsuda, T. Kawabata, Y. Uetani, T. Sato, A. Kamio, and S. Ikeno: *Mater. Sci. Forum*, 2000, vols. 331–337, pp. 989-94.
4. M. Murayama and K. Hono: *Acta Mater.*, 1999, vol. 47 (5), pp. 1537-48.
5. K. Matsuda, Y. Sakaguchi, Y. Miyata, Y. Uetani, T. Sato, A. Kamio, and S. Ikeno: *J. Mater. Sci.*, 2000, vol. 35, pp. 179-89.
6. K. Matsuda, S. Ikeno, T. Sato, and A. Kamio: *Scripta Mater.*, 1996, vol. 34 (11), pp. 1797-1802.
7. A. Frøseth: Ph.D. Thesis, Norwegian University of Science and Technology, Trondheim, 2003, pp. 63-111.
8. A. Frøseth, R. Høier, P.M. Derlet, S.J. Andersen, and C.D. Marioara: *Phys. Rev. B.*, 2003, vol. 67, p. 224106.
9. C.D. Marioara, S.J. Andersen, J. Jansen, and H.W. Zandbergen: *Acta Mater.*, 2003, vol. 51 (3), pp. 789-96.
10. S.J. Andersen: *Metall. Mater. Trans. A*, 1995, vol. 26A, pp. 1931-38.
11. O.R. Myhr, Ø. Grong, and S.J. Andersen: *Acta Mater.*, 2001, vol. 49, pp. 65-75.
12. S.J. Andersen, H.W. Zandbergen, J. Jansen, C. Traeholt, U. Tundal, and O. Reiso: *Acta Mater.*, 1998, vol. 46 (9), pp. 3283-98.
13. P.M. Derlet, S.J. Andersen, C.D. Marioara, and A. Frøseth: *J. Phys. Cond. Matter*, 2002, vol. 14, pp. 4011-24.
14. P. Donnadieu: *Phil. Mag. A*, 1999, vol. 79 (6), p. 1347.
15. C.D. Marioara, S.J. Andersen, J. Jansen, and H.W. Zandbergen: *Acta Mater.*, 2001, vol. 49, pp. 321-28.
16. A. Kelly and R.B. Nicholson: *Progr. Mater. Sci.*, 1963, vol. 10, p. 151.
17. S.J. Andersen, C.D. Marioara, A. Froseth, and R. Vissers: *Mater. Sci. Eng. A*, 2005, vol. 390/1–2, pp. 127-38.